Phase diagram of infinite layer praseodymium nickelate $Pr_{1-x}Sr_xNiO_2$ thin films

Motoki Osada [1,2,3,*], Bai Yang Wang [1,4] Kyuho Lee [1,4] Danfeng Li [1,2,5,†] and Harold Y. Hwang [1,2,‡]

[1]*Stanford Institute for Materials and Energy Sciences, SLAC National Accelerator Laboratory, Menlo Park, California 94025, USA*
[2]*Department of Applied Physics, Stanford University, Stanford, California 94305, USA*
[3]*Department of Materials Science and Engineering, Stanford University, Stanford, California 94305, USA*
[4]*Department of Physics, Stanford University, Stanford, California 94305, USA*
[5]*Department of Physics, City University of Hong Kong, Kowloon, Hong Kong, People's Republic of China*

We report the phase diagram of infinite layer $Pr_{1-x}Sr_xNiO_2$ thin films synthesized via topotactic reduction from the perovskite precursor phase using CaH_2. Based on the electrical transport properties, we find a doping-dependent superconducting dome extending between $x = 0.12$ and 0.28 with a maximum superconducting transition temperature T_c of 14 K at $x = 0.18$, bounded by weakly insulating behavior on both sides. In contrast to the narrower dome observed in $Nd_{1-x}Sr_xNiO_2$, a local T_c suppression near $x = 0.2$ was not observed for the $Pr_{1-x}Sr_xNiO_2$ system. Normal-state Hall effect measurements indicate mixed carrier contributions of both electrons and holes and show a sign change in the Hall coefficient as functions of temperature and x, quite similar to that in $Nd_{1-x}Sr_xNiO_2$. Also similar is the observation of a minimum in the normal-state resistivity associated with the superconducting compositions. These findings indicate an infinite layer nickelate phase diagram that is relatively insensitive to the rare-earth element but suggest that disorder arising from the variations of the ionic radii on the rare-earth site affects the superconducting dome.

High-T_c cuprates are unusual materials systems, marked by a rather complex phase diagram enriched with intertwined electronic orders [1,2]. Despite exhibiting a generic doping-dependent phase diagram with common features, which many consider a hallmark of the physics of the CuO_2 planes [1], cuprates of various crystal structures [3–7] show rather diverse properties, manifested by different configurations of Cu-O stacking layers [8–10], a remarkably wide range of transition temperatures [1], and varied strength of coupling to proximate competing orders [2,11]. Many of these aspects represent the intimate interplay between the local chemical environment [10], partially set by the cation sublattices outside the Cu-O networks [12–14], and the macroscopic materials properties. Examples include the famous stripe phase [2,15,16] induced by the local instability of the lattice distortion via cation substitution, such as $La_{2-x}Ba_xCuO_4$ [17] and Nd- or Eu-substituted $La_{2-x}Sr_xCuO_4$ [15,18], the latter of which involves a direct tuning of the chemical pressure by varying the rare-earth elements. Such lattice distortion derived rare-earth dependence was also clearly seen in the perovskite nickelates ($ANiO_3$) [19,20], marked by their A-site dependent metal-insulator transition and charge-disproportionation temperatures. Furthermore, a rare-earth dependent ground state has been found in the trilayer nickelates with square-planar coordination in which the role of the lanthanide elements remains elusive [21].

The recent observation of superconductivity in rare-earth infinite layer nickelates [22,23] has stimulated the discussion on the relationship to their cuprate counterparts in that they share the same atomic structure and starting $3d^9$ electronic configuration, yet perhaps hosting distinct electronic structures and low-energy physics with a multiorbital nature as noted by Lee and Pickett [24]. More recent theoretical considerations [25–31] and scattering/spectroscopic experiments [32,33] highlight the unusual role of rare-earth orbitals and their interaction and hybridization. This raises the question of whether the nickelate superconductors are close cousins to the heavy fermion superconductors [34–36] or intermetallic superconductors, such as $RENi_2B_2C$ (RE = rare-earth) [37]. The latter family of compounds shows a strong dependence of magnetic ordering and superconductivity on the lanthanide element [38] in which the two phenomena seem to correlate. However, superconductivity with similar T_c values observed in thin film $Nd_{0.8}Sr_{0.2}NiO_2$ [22] and $Pr_{0.8}Sr_{0.2}NiO_2$ [23] suggests that the emergence of superconductivity seems relatively insensitive to the details of the rare-earth $4f$ electron configuration [39–41]. In this regard, the question of whether these doped infinite layer nickelate superconductors host mixed aspects [40,42–45] of both cuprates and superconductors with hybridized rare-earth contributions calls for further investigation.

With this notion, and motivated by the observation of a doping-dependent superconducting dome in thin-film $Nd_{1-x}Sr_xNiO_2$ [46,47], we have investigated the phase diagram across a series of $Pr_{1-x}Sr_xNiO_2$ ($0 \leqslant x \leqslant 0.32$) thin films. We report a superconducting dome structure in the phase diagram of the $Pr_{1-x}Sr_xNiO_2$ family with a maximum

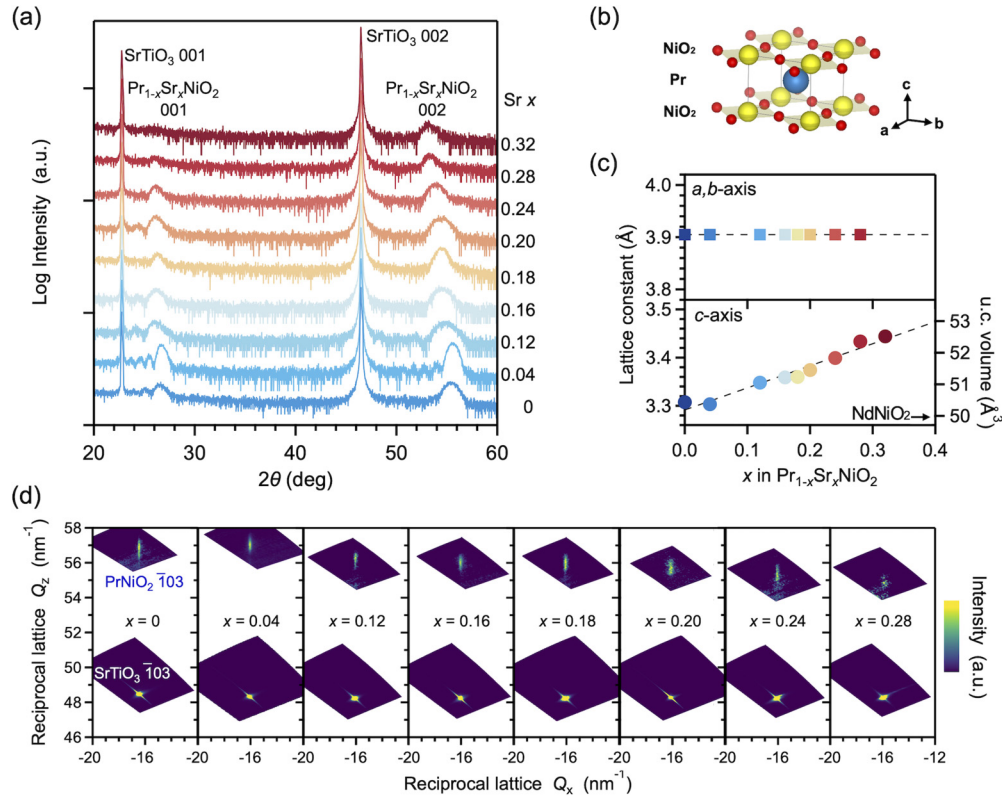*mosada@stanford.edu
†danfeng.li@cityu.edu.hk
‡hyhwang@stanford.edu

FIG. 1. (a) X-ray diffraction θ-2θ symmetric scans of $Pr_{1-x}Sr_xNiO_2$ thin films grown on $SrTiO_3$ (001) substrates. (b) The atomic structure of the infinite-layer $PrNiO_2$. (c) Lattice constants and unit-cell volumes of $Pr_{1-x}Sr_xNiO_2$ thin films. The unit-cell volume of thin-film $NdNiO_2$ is shown as a reference [46]. (d) Reciprocal space maps around the $\bar{1}03$ peaks. All scans were performed at room temperature.

T_c of 14 K at $x = 0.18$. We show that superconductivity is bound by $x = 0.12$ and 0.28, beyond which the system exhibits weakly insulating behavior at low temperatures at both ends of the superconducting dome. Although the behavior across the different phase boundaries is in qualitative resemblance to that in the Nd series, the fine structure of the superconducting dome shows rather different features, namely, the absence of the T_c suppression observed in $Nd_{1-x}Sr_xNiO_2$ and a broader superconducting doping range. Nevertheless, the Hall effect data in both systems show quantitatively very similar trends, marked by continuous zero crossings of the Hall coefficient (R_H) in temperature and doping. These data indicate the band configuration and Fermi-surface structure are likely somewhat insensitive to the rare-earth site, consistent with density functional theory calculations [39,40].

$Pr_{1-x}Sr_xNiO_2$ films of 6.3–9.7 nm in thickness were grown by pulsed laser deposition, followed by a subsequent topotactic reduction reaction, using the same conditions as described previously [23]. In that study, we found that an upper $SrTiO_3$ (STO) capping layer was not essential for stabilizing a uniform single-crystalline infinite layer structure in $PrNiO_2$ and $Pr_{0.8}Sr_{0.2}NiO_2$ thin films, which can be possibly attributed to a larger tolerance factor and a better lattice matching to the STO substrate. Therefore, the $Pr_{1-x}Sr_xNiO_3$ films were synthesized without a $SrTiO_3$ capping layer. The substrate temperature was kept at $570\,^\circ$C. The laser fluence and oxygen pressure for the growth of undoped $PrNiO_3$ and doped $Pr_{1-x}Sr_xNiO_3$ ($x \neq 0$) are 1.39 J/cm^2, 200 mTorr and

2.19 J/cm^2, 250 mTorr, respectively. The laser repetition was 4 Hz for all samples. The x-ray diffraction (XRD) characterization and transport measurements were performed as described previously [23].

High-quality precursor $Pr_{1-x}Sr_xNiO_3$ films were synthesized, which facilitates a successful topotactic transition to the resultant infinite layer $Pr_{1-x}Sr_xNiO_2$. In this way, the wide sample-to-sample variation in the temperature-dependent resistivity $\rho_{xx}(T)$, pertaining to $Nd_{1-x}Sr_xNiO_2$ [22,48], is quite a bit narrowed here. Based on this, for simplicity, throughout this Rapid Communication we show one dataset of representative samples for each doping level. Figure 1 illustrates the structural properties of the representative $Pr_{1-x}Sr_xNiO_2$ thin films for each x, characterized by XRD measurements. Across all x, we observe clear film peaks in the symmetric θ-2θ scans [Fig. 1(a)] corresponding to the infinite layer phase, which has reduced lattice parameters along the c axis as compared to the perovskite precursor phase [Fig. 1(b)]. The decreasing trend of the 001 peak intensity with Sr substitution is consistent with our calculation of the powder-diffraction pattern in $Pr_{1-x}Sr_xNiO_2$ (not shown) where the ratio of 001 peak intensity to 002 peak intensity is 0.44 at $x = 0$ and monotonically decreases to 0.22 at $x = 0.32$. This structure factor variation due to Sr substitution should be accounted for when considering the overall lower 001 peak intensity upon increasing x. Although varied in intensity, the positions of the film peaks clearly shift to a lower angle as x increases, consistent with a monotonic increase of the c-axis lattice constants in the range from 3.31 Å ($x = 0$) to 3.44 Å ($x = 0.32$) [Fig. 1(c)].
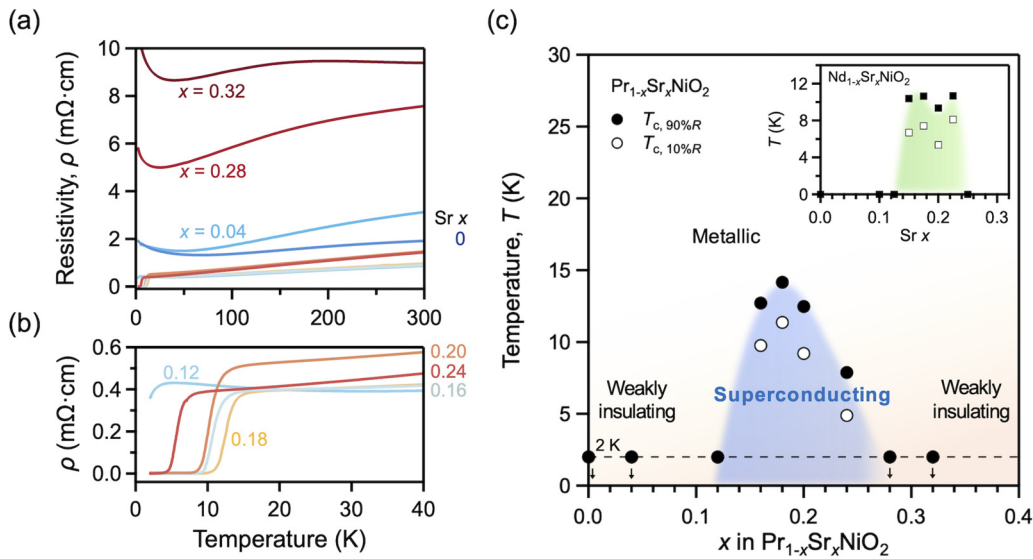
FIG. 2. (a) Representative temperature dependence of resistivity ρ-T curves for $Pr_{1-x}Sr_xNiO_2$ thin films. (b) The enlarged ρ-T curves in the temperature range from 2 to 40 K. (c) The phase diagram of $Pr_{1-x}Sr_xNiO_2$ thin films. Closed and open circles represent $T_{c, 90\%R}$ and $T_{c, 10\%R}$ as defined to be the temperatures at which the resistivity is 90% and 10% of the resistivity value at 20 K, respectively. The dashed line indicates the minimum measurement temperature 2 K. The inset shows the phase diagram of $Nd_{1-x}Sr_xNiO_2$ thin films adapted from Ref. [46].

Reciprocal space maps around the $\bar{1}03$ diffraction peak [Fig. 1(d)] confirm that the films are in all cases strained to the substrate. Consequently, the a-axis lattice constants match that for STO, which is 3.91 Å [Fig. 1(c)]. The calculated unit-cell volume of $PrNiO_2$ is slightly larger than that of the thin-film $NdNiO_2$ on STO [46], the value of which is indicated as a reference in Fig. 1(c). These are in line with the fact that the ionic radius of Pr^{3+} (113 pm) is larger than Nd^{3+} (111 pm) in the same crystal environment and closer to that of Sr^{2+} (126 pm) [49].

The temperature-dependent resistivity $\rho_{xx}(T)$ for thin-film $Pr_{1-x}Sr_xNiO_2$ down to 2 K is presented in Figs. 2(a) and 2(b). For both the under- and overdoped regimes ($x = 0, 0.04, 0.28$, and 0.32), ρ_{xx} shows a minimum around a temperature T_{min} of 70, 45, 25, and 40 K, respectively, below which an upturn appears. Despite having a smaller T_{min} with respect to the undoped case, the overall resistivity for $x = 0.28$ and 0.32 is much larger, and their temperature dependence above T_{min} deviates from the remaining curves. This high ρ_{xx}, together with the reduced (001) peak intensity seen in the XRD scans [Fig. 1(a)], suggests that both structural and electronic disorders induced by Sr doping may contribute in the overdoped regime. In the intermediate doping levels, i.e., $x = 0.16, 0.18, 0.20$, and 0.24, all resistivity curves show metallic behavior with a roughly linear temperature dependence approximately above T_c, a hallmark of cuprates and organic superconductors [1,11]. At lower temperature, superconducting transitions with zero resistance states are observed [Fig. 2(b)]. One peculiar doping point is $x = 0.12$ where both a low-temperature resistivity upturn and onset of superconductivity are present, demarking the edge of the superconducting dome. From $\rho_{xx}(T)$, we construct a superconducting phase diagram as shown in Fig. 2(c) where transition temperatures $T_{c,90\%R}$ and $T_{c,10\%R}$ are defined as the temperature at which the resistivity is 90% and 10% of $\rho_{xx}(T = 20\,K)$, respectively. The doping-dependent superconducting dome

spans across $0.12 \leqslant x \leqslant 0.24$ with the maximum $T_{c, 90\%R}$ of 14 K at $x = 0.18$. This dome is somewhat wider than that of the $Nd_{1-x}Sr_xNiO_2$ system ($0.15 \leqslant x \leqslant 0.225$) [46] as shown in the inset of Fig. 2(c). Furthermore, the dome [or the functional form of $T_c(x)$] is more of a "bell" shape. Around the optimal doping level ($x = 0.18$), T_c is higher and the transition width (difference between $T_{c,90\%R}$ and $T_{c,10\%R}$) is arguably narrower, as compared to that of $Nd_{1-x}Sr_xNiO_2$. All of these aspects likely reflect that $Pr_{1-x}Sr_xNiO_2$ films are generally of higher stability and crystallinity [23]. We also note that the small suppression of T_c observed in the $Nd_{1-x}Sr_xNiO_2$ system is absent here and discussed further below.

The normal state Hall coefficient R_H ($0.12 \leqslant x \leqslant 0.32$) is shown in Fig. 3(a) as a function of temperature. The Hall
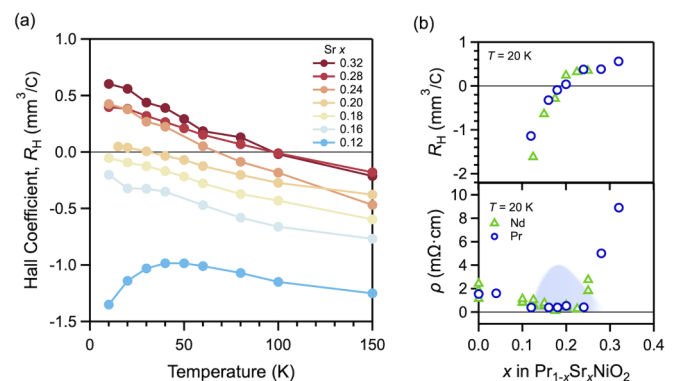

FIG. 3. (a) Normal-state Hall coefficient as a function of temperature for $Pr_{1-x}Sr_xNiO_2$ thin films. (b) Hall coefficient R_H and resistivity ρ as a function of Sr x at 20 K (top and bottom, respectively). Triangles and circles represent $Nd_{1-x}Sr_xNiO_2$ [46] and $Pr_{1-x}Sr_xNiO_2$, respectively. The superconducting dome of $Pr_{1-x}Sr_xNiO_2$ thin films is shown in the background of the lower panel.

resistivity ρ_{yx} shows linear magnetic field ($\mu_0 H$) dependence up to 8 T. For all doping levels presented here, R_H increases with decreasing temperature, except for $x = 0.12$, where the R_H maximum associated with $T_{\min}$ is present. In particular, the negative $R_H(T)$ for $x = 0.12$ is consistent with the prediction of partially occupied Pr $5d$ derived states [39]. For samples with higher doping ($x \geqslant 0.20$), $R_H(T)$ crosses zero in a continuous manner, suggesting the mixed carrier contribution of electrons and holes. This multiorbital nature is also corroborated by the smooth sign change in R_H as function of x, for instance, at $T = 20$ K as shown in the top panel of Fig. 3(b), corresponding to an increasing depletion of the electron pockets primarily composed of Pr $5d$ bands [39,40] or a change in the Fermi-surface topology upon doping close to half-filling in the strong correlation limit [50].

It is intriguing to see that superconductivity is associated with a small R_H proximate to zero but of either sign [Fig. 3(b); top panel], and the minimum in the normal state ρ_{xx} [Fig. 3(b); bottom panel], both of which are plotted in comparison to the similar dataset obtained for Nd$_{1-x}$Sr$_x$NiO$_2$ [46]. In particular, the enhanced stability of Pr$_{1-x}$Sr$_x$NiO$_2$ allowed us to explore deeper into the heavily doped side of the phase diagram and access the more resistive regime where both the systematic behavior of R_H and the "V-shape" normal-state $\rho_{xx}(x)$ (with larger scale) persist.

We now discuss the implications of our results. First, our observation of a T_c dome with similar doping dependence and the universal trend of R_H in temperature and doping in both Pr$_{1-x}$Sr$_x$NiO$_2$ and Nd$_{1-x}$Sr$_x$NiO$_2$ suggests phenomenologically similar electronic structure [35,36] for both cases. These findings warrant further experimental investigations of the Fermi surface and the band structure, ideally using techniques, such as angle-resolved photoemission spectroscopy if experimentally accessible. Next, the absence of the dip in T_c in the superconducting dome of Pr$_{1-x}$Sr$_x$NiO$_2$ does not seem to support the existence of a universal "anomalous" doping level x (0.2 for Nd$_{1-x}$Sr$_x$NiO$_2$) across different nickelate materials. Instead, if such a local suppression of superconductivity is considered suggestive of stripe order as widely seen in cuprates [2,15,17] and other nickelates [51–53], our findings indicates that small differences in strain field or chemical pressure, can affect the ground state of the system. This could be analogous to the different scale of the "1/8" anomaly in La$_{2-x}$Sr$_x$CuO$_4$ [54], La$_{2-x}$Ba$_x$CuO$_4$ [17], and Nd- or Eu-substituted La$_{2-x}$Sr$_x$CuO$_4$ [15,18], and the general role of cation size disorder in determining T_c [13]. Although these interpretations are yet to be experimentally established, our results thus far provide evidence that the infinite layer

nickelates are susceptible to the delicate balance between the local chemical environment and electronic correlations.

It should be noted that as we approach the largest values of Sr substitution x in the heavily doped regime, the materials pose increasingly significant challenges to materials synthesis. First, this is because the formal valence of Ni (Ni^{3+x}) in the precursor perovskite phase deviates further away from its most thermodynamically stable state (Ni^{2+}), which can drive the formation of extended defects to perturb the local Ni valence [48]. In addition, Sr substitution introduces cation-site disorder as indicated by the systematic reduction of 001 peak intensity as x increases [Fig. 1(a)]. As a consequence, systematic contributions from materials imperfections to ρ_{xx} will likely grow with increasing x. In this regard, further careful optimization of growth and investigation of the defect structure, such as the Ruddlesden-Popper-type faults that were observed in Nd$_{1-x}$Sr$_x$NiO$_2$ thin films [46,48], in the heavily doped regime is required. However, considering the clear trend in the doping-dependent T_c and R_H, our finding of a superconducting dome associated with a continuous evolution of the electronic structure with multiband character should be qualitatively robust.

To summarize, we have extended the study of the phase diagram of the infinite layer nickelates, analogous to cuprate systems, by replacing Nd with Pr. Given the greater lattice stability of the precursor perovskite phase Pr$_{1-x}$Sr$_x$NiO$_3$ due to the larger tolerance factor and smaller lattice mismatch to STO in the perovskite phase [23] with respect to the previously studied Nd$_{1-x}$Sr$_x$NiO$_3$, we were able to stabilize a series of samples to higher doping levels. We observed a T_c dome bound by $x = 0.12$ and 0.28 in the phase diagram of Pr$_{1-x}$Sr$_x$NiO$_2$, beyond which the system exhibits low-temperature weakly insulating behavior at both ends of the doping levels studied here. R_H displays zero-crossing behavior both as a function of temperature and doping, qualitatively in agreement with a multiband Fermi surface and quantitatively similar to Nd$_{1-x}$Sr$_x$NiO$_2$. A continuous variation of T_c with a single maximum of 14 K at $x = 0.18$ and a larger doping range for superconductivity were additionally found, which indicates that cation size disorder effects may play a role in the detailed structure of the superconducting dome.

[1] B. Keimer, S. A. Kivelson, M. R. Norman, S. Uchida, and J. Zaanen, Nature (London) **518**, 179 (2015).

[2] E. Fradkin, S. A. Kivelson, and J. M. Tranquada, Rev. Mod. Phys. **87**, 457 (2015).

[3] J. G. Bednorz and K. A. Müller, Z. Phys. B **64**, 189 (1986).

[4] M. K. Wu, J. R. Ashburn, C. J. Torng, P. H. Hor, R. L. Meng, L. Gao, Z. J. Huang, Y. Q. Wang, and C. W. Chu, Phys. Rev. Lett. **58**, 908 (1987).

[5] Y. Tokura, H. Takagi, and S. Uchida, Nature (London) **337**, 345 (1989).

[6] H. Sawa, S. Suzuki, M. Watanabe, J. Akimitsu, H. Matsubara, H. Watabe, S. Uchida, K. Kokusho, H. Asano, F. Izumi, and E. Takayama-Muromachi, Nature (London) **337**, 347 (1989).

[7] M. G. Smith, A. Manthiram, J. Zhou, J. B. Goodenough, and J. T. Markert, Nature (London) **351**, 549 (1991).

[8] B. A. Scott, E. Y. Suard, C. C. Tsuei, D. B. Mitzi, T. R. McGuire, B.-H. Chen, and D. Walker, Physica C **230**, 239 (1994).

[9] A. Iyo, Y. Tanaka, H. Kito, Y. Kodama, P. M. Shirage, D. D. Shivagan, H. Matsuhata, K. Tokiwa, and T. Watanabe, J. Phys. Soc. Jpn. **76**, 094711 (2007).

[10] H. Eisaki, N. Kaneko, D. L. Feng, A. Damascelli, P. K. Mang, K. M. Shen, Z.-X. Shen, and M. Greven, Phys. Rev. B **69**, 064512 (2004).

[11] L. Taillefer, Annu. Rev. Condens. Matter Phys. **1**, 51 (2010).

[12] S. Raghu, R. Thomale, and T. H. Geballe, Phys. Rev. B **86**, 094506 (2012).

[13] J. P. Attfield, A. L. Kharlanov, and J. A. McAllister, Nature (London) **394**, 157 (1998).

[14] K. Fujita, T. Noda, K. M. Kojima, H. Eisaki, and S. Uchida, Phys. Rev. Lett. **95**, 097006 (2005).

[15] J. M. Tranquada, B. J. Sternlieb, J. D. Axe, Y. Nakamura, and S. Uchida, Nature (London) **375**, 561 (1995).

[16] S. A. Kivelson, I. P. Bindloss, E. Fradkin, V. Oganesyan, J. M. Tranquada, A. Kapitulnik, and C. Howald, Rev. Mod. Phys. **75**, 1201 (2003).

[17] M. Fujita, H. Goka, K. Yamada, J. M. Tranquada, and L. P. Regnault, Phys. Rev. B **70**, 104517 (2004).

[18] J. Fink, E. Schierle, E. Weschke, J. Geck, D. Hawthorn, V. Soltwisch, H. Wadati, H.-H. Wu, H. A. Dürr, N. Wizent, B. Büchner, and G. A. Sawatzky, Phys. Rev. B **79**, 100502(R) (2009).

[19] S. Middey, J. Chakhalian, P. Mahadevan, J. W. Freeland, A. J. Millis, and D. D. Sarma, Annu. Rev. Mater. Res. **46**, 305 (2016).

[20] S. Catalano, M. Gibert, J. Fowlie, J. Íñiguez, J.-M. Triscone, and J. Kreisel, Rep. Prog. Phys. **81**, 046501 (2017).

[21] J. Zhang, A. S. Botana, J. W. Freeland, D. Phelan, H. Zheng, V. Pardo, M. R. Norman, and J. F. Mitchell, Nat. Phys. **13**, 864 (2017).

[22] D. Li, K. Lee, B. Y. Wang, M. Osada, S. Crossley, H. R. Lee, Y. Cui, Y. Hikita, and H.Y. Hwang, Nature (London) **572**, 624 (2019).

[23] M. Osada, B. Y. Wang, B. H. Goodge, K. Lee, H. Yoon, K. Sakuma, D. Li, M. Miura, L. F. Kourkoutis, and H. Y. Hwang, Nano Lett. **20**, 5735 (2020).

[24] K.-W. Lee and W. E. Pickett, Phys. Rev. B **70**, 165109 (2004).

[25] A. S. Botana and M. R. Norman, Phys. Rev. X **10**, 011024 (2020).

[26] M. Hirayama, T. Tadano, Y. Nomura, and R. Arita, Phys. Rev. B **101**, 075107 (2020).

[27] X. Wu, D. Di Sante, T. Schwemmer, W. Hanke, H. Y. Hwang, S. Raghu, and R. Thomale, Phys. Rev. B **101**, 060504(R) (2020).

[28] S. Ryee, H. Yoon, T. J. Kim, M. Y. Jeong, and M. J. Han, Phys. Rev. B **101**, 064513 (2020).

[29] P. Jiang, L. Si, Z. Liao, and Z. Zhong, Phys. Rev. B **100**, 201106(R) (2019).

[30] F. Lechermann, Phys. Rev. B **101**, 081110(R) (2020).

[31] J. Karp, A. S. Botana, M. R. Norman, H. Park, M. Zingl, and A. Millis, Phys. Rev. X **10**, 021061 (2020).

[32] M. Hepting, D. Li, C. J. Jia, H. Lu, E. Paris, Y. Tseng, X. Feng, M. Osada, E. Been, Y. Hikita, Y.-D. Chuang, Z. Hussain, K. J. Zhou, A. Nag, M. Garcia-Fernandez, M. Rossi, H. Y. Huang, D. J. Huang, Z. X. Shen, T. Schmitt, H. Y. Hwang, B. Moritz, J. Zaanen, T. P. Devereaux, and W. S. Lee, Nature Mater. **19**, 381 (2020).

[33] B. H. Goodge, D. Li, M. Osada, B. Y. Wang, K. Lee, G. A. Sawatzky, H. Y. Hwang, and L. F. Kourkoutis, arXiv:2005.02847.

[34] G. R. Stewart, Rev. Mod. Phys. **56**, 755 (1984).

[35] C. Pfleiderer, Rev. Mod. Phys. **81**, 1551 (2009).

[36] Q. Si and F. Steglich, Science **329**, 1161 (2010).

[37] R. J. Cava, H. Takagi, H. W. Zandbergen, J. J. Krajewski, W. F. Peck, Jr., T. Siegrist, B. Batlogg, R. B. van Dover, R. J. Felder, K. Mizuhashi, J. O. Lee, H. Eisaki, and S. Uchida, Nature (London) **367**, 252 (1994).

[38] Z. Zeng, D. Guenzburger, D. E. Ellis, and E. M. Baggio-Saitovitch, Physica C **271**, 23 (1996).

[39] E. Been, W.-S. Lee, H. Y. Hwang, Y. Cui, J. Zaanen, T. Devereaux, B. Moritz, and C. Jia, arXiv:2002.12300.

[40] J. Kapeghian and A. S. Botana, Phys. Rev. B **102**, 205130 (2020).

[41] M.-Y. Choi, K.-W. Lee, and W. E. Pickett, Phys. Rev. B **101**, 020503(R) (2020).

[42] Y. Nomura, M. Hirayama, T. Tadano, Y. Yoshimoto, K. Nakamura, and R. Arita, Phys. Rev. B **100**, 205138 (2019).

[43] H. Sakakibara, H. Usui, K. Suzuki, T. Kotani, H. Aoki, and K. Kuroki, Phys. Rev. Lett. **125**, 077003 (2020).

[44] Y.-H. Zhang and A. Vishwanath, Phys. Rev. Research **2**, 023112 (2020).

[45] H. Zhang, L. Jin, S. Wang, B. Xi, X. Shi, F. Ye, and J.-W. Mei, Phys. Rev. Research **2**, 013214 (2020).

[46] D. Li, B. Y. Wang, K. Lee, S. P. Harvey, M. Osada, B. H. Goodge, L. F. Kourkoutis, and H. Y. Hwang, Phys. Rev. Lett. **125**, 027001 (2020).

[47] S. Zeng, C. S. Tang, X. Yin, C. Li, M. Li, Z. Huang, J. Hu, W. Liu, G. J. Omar, H. Jani, Z. S. Lim, K. Han, D. Wan, P. Yang, S. J. Pennycook, A. T. S. Wee, and A. Ariando, Phys. Rev. Lett. **125**, 147003 (2020).

[48] K. Lee, B. H. Goodge, D. Li, M. Osada, B. Y. Wang, Y. Cui, L. F. Kourkoutis, and H. Y. Hwang, APL Mater. **8**, 041107 (2020).

[49] R. D. Shannon, Acta Crystallogr., Sect. A: Cryst. Phys., Diffr., Theor. Gen. Crystallogr. **A32**, 751 (1976).

[50] W. O. Wang, J. K. Ding, B. Moritz, E. W. Huang, and T. P. Devereaux, npj Quantum Mater. **5**, 51 (2020).

[51] J. Zhang, Y.-S. Chen, D. Phelan, H. Zheng, M. R. Norman, and J. F. Mitchell, Proc. Natl. Acad. Sci. USA **113**, 8945 (2016).

[52] J. Zhang, D. M. Pajerowski, A. S. Botana, H. Zheng, L. Harriger, J. Rodriguez-Rivera, J. P. C. Ruff, N. J. Schreiber, B. Wang, Y.-S. Chen, W. C. Chen, M. R. Norman, S. Rosenkranz, J. F. Mitchell, and D. Phelan, Phys. Rev. Lett. **122**, 247201 (2019).

[53] J. M. Tranquada, D. J. Buttrey, V. Sachan, and J. E. Lorenzo, Phys. Rev. Lett. **73**, 1003 (1994).

[54] H. Takagi, T. Ido, S. Ishibashi, M. Uota, S. Uchida, and Y. Tokura, Phys. Rev. B **40**, 2254 (1989).